eprints@whiterose.ac.uk
https://eprints.whiterose.ac.uk/

Full Length Article

Simulation and modelling study of a chemical absorption plant to evaluate capture effectiveness when treating high CO_2 content iron and steel industry emissions

Jack Wells [a,*], Andy Heeley [b], Muhammad Akram [a,b], Kevin J. Hughes [a], Derek B. Ingham [a], Mohamed Pourkashanian [a,b]

[a] *Energy 2050, Department of Mechanical Engineering, University of Sheffield, Sheffield, South Yorkshire S3 7RD, United Kingdom*
[b] *Translational Energy Research Centre, Sheffield Business Park, Europa Avenue, Sheffield, South Yorkshire S9 1ZA, United Kingdom*

ABSTRACT

Humanity must decarbonise to prevent climate disaster associated with CO_2 and other greenhouse gases. The iron and steel industry contribute significantly to global CO_2, with 70 % of integrated steel plant emissions arising from the blast furnace. Green alternatives to blast furnaces are still in development, requiring an intermediate stepping-stone solution to begin the decarbonisation journey. Chemical absorption using amine solvents is a proven carbon capture technology, theoretically ideal for flue gas CO_2 concentrations and conditions typical of iron and steel making industrial processes. A representative simulation of the Translational Energy Research Centre (TERC) pilot-scale amine capture plant (ACP) was developed in Aspen Plus V11.0 and identified conditions to minimise the specific reboiler duty (SRD) for representative gases of the iron and steel industry. This work predicted operating conditions and trends when using a monoethanolamine (MEA) solvent concentration of 35 wt% across flue gas CO_2 concentrations up to 25 mol% CO_2.

This work established that optimal L/G and solvent/CO_2 ratios for MEA absorption systems can be predicted through knowledge of the flue gas CO_2 concentration and the desired capture efficiency of the system alone, without consideration of the volumetric gas flow rate of the system. For flue gas CO_2 concentrations of 10 to 25 mol%, optimal L/G ratios of 2.5 to 4.6 and solvent/CO_2 ratios of 17.1 to 13.5 were identified to achieve 90 % capture efficiency, with the optimal L/G ratio increasing by approximately 0.7 for each 5 mol% increase of CO_2 concentration. Optimal lean solvent loadings ranged from 0.245 to 0.294 mol·CO_2/mol·MEA, with rich solvent loadings ranging from 0.500 to 0.517 mol·CO_2/mol·MEA. Solvent capacities proved instrumental in understanding the relationship between optimal solvent flow rate and flue gas CO_2 concentration for different capture efficiencies.

Temperature profile assessment of absorbing and stripping columns is crucial to optimise the system, as each column exhibits unique operational behaviours, with additional attention given to the cross-heat exchanger. The results illustrate key parameters and considerations for CO_2 capture of the iron and steel industry, providing initial setpoint conditions and guidance for optimisation. The developed simulation model can be calibrated to represent other MEA absorption systems.

1. Introduction

It is undeniable that human activity in the post-industrialisation era is a primary contributor to the rapid increase in global atmospheric CO_2 concentration [1]. Increasing greenhouse gas (GHG) emissions, including CO_2, are having significant effects on the Earth's atmosphere, leading to rising global temperatures and devastating climate change

[2]. It is a challenge for humanity to prevent, or at least minimise and mitigate these greenhouse gas emissions to avert further climate impacts and safeguard future generations from climate disaster [3].

Optimistic targets have been set in local legislation and global agreements to achieve significant decarbonisation worldwide [4–7], with different economic sectors each having unique challenges and approaches to reducing carbon emissions [8]. Within the industrial sector,

iron and steelmaking currently accounts for 11 % of the total global CO_2 emissions [9,10], when considering direct and indirect emissions for steel production. Mitigating these significant emissions must be achieved as part of industrial decarbonisation efforts [9].

From 2012 to 2021, global production of crude steel has increased from 1.56 billion to 1.96 billion metric tonnes [11]. 70.8 % of global crude steel production in 2021 relied upon conventional coal-based blast furnaces as the principal liquid iron manufacturing process. China produces over half of the world's steel supply with nearly 90 % of this supply from the blast furnace route [11]. Blast furnaces are responsible for around 70 % of an integrated steel mill's CO_2 emissions [12], with a concentration ranging from 20 to 25 mol% CO_2 in the flue gas [13]. Steel industry decarbonisation efforts should focus on reducing emissions from the blast furnace to achieve maximum impact [12].

The long-term future of green steel production will likely remove blast furnaces entirely and rely on hydrogen-based direct reduced iron (DRI) reactors for liquid iron production. Green hydrogen for the DRI process would be produced through electrolysis using renewable energy, achieving CO_2 reductions of over 95 % [14,15]. However, the global hydrogen economy has its own challenges, scaling up green hydrogen production and rolling out supply chains will take time [16,17]. Even if the hydrogen economy improves, blast furnaces have long design lifetimes of up to 25 years [18,19], with 71 % of the existing fleet needing major refurbishment by 2030, and the remainder by 2040 [20]. Consequently, many blast furnaces will continue operation for several decades before needing replacement.

An intermediate solution is required to decarbonise existing conventional blast furnaces to provide a transitional technology step between the existing process and potential green manufacturing process. Carbon Capture and Storage (CCS), which has been described by the International Energy Agency (IEA) as a key component to achieve deep carbon emission reductions for the iron and steel industry [21–23] will probably provide an interim solution for foundation industries [24]. Chemical absorption technologies are the most well-developed CCS options suitable for the capture of steel making emissions. Not only is CCS the most proven technology due to its maturity as a gas capture process and widespread research but typical process emissions from steelmaking have ideal pressures, temperatures, and CO_2 concentrations for chemical absorption [25–28]. Several studies have been conducted in this area to assess the feasibility of developing such a system for the iron and steel industry. Arasto et al. [29] used monoethanolamine (MEA) solvent in a modelling assessment of hypothetical cases of a real steel plant in 2012 and concluded that the solution is technically feasible. From 2014 to 2018, the VALORCO project led by ArcelorMittal investigated capturing CO_2 from blast furnaces using chemical absorption [30]. This involved studies conducted by Dreillard et al. [31] from lab scale to mini-pilot scale using three different solvents: Hicapt™ process (MEA 30 wt%), Hicapt+™ process (MEA 40 wt%) and DMX™ process (Demixing solvent). Solvent degradation with blast furnace gas was considered negligible in these trials, concluding that the technology is promising and needs demonstrating on an industrial scale pilot plant. More recently in 2021, Carbon Clean commissioned the world's first carbon capture plant that captures directly from blast furnace gas for Tata Steel in Jamshedpur [32,33], capturing five tonnes of CO_2 per day using amine-based proprietary solvents. These studies demonstrated promising developments in pilot application of the technology, but further studies are required to widen the knowledge base and reduce the investment risk of chemical absorption technology, thereby increasing the uptake of CCS.

The Translational Energy Research Centre (TERC) based in Sheffield, United Kingdom, is home to an industrial pilot-scale amine capture plant (ACP) designed for post-combustion capture [34,35]. The pilot plant is capable of capturing approximately one tonne of CO_2 per day, dealing with gas flows up to 210 Nm^3/h, and can achieve > 95 % capture efficiencies using monoethanolamine (MEA) under certain conditions.

Historically, this plant has been used for process optimisation,

solvent degradation studies, solvent development testing and aerosol emissions control [36–40]. The ACP was initially designed for coal combustion flue gas before existing coal-fired power stations began to close [36], with subsequent projects not requiring flue gas flows of CO_2 concentration significantly higher than 10 mol%. This presents a unique opportunity to investigate the ACP's capability to achieve deep cleaning of gases that are typical of the iron and steel industry, examples of which have typical compositions presented in Table 1, ignoring trace compounds [41,42].

The operation of the ACP with high CO_2 concentration gases has been evaluated using Aspen Plus V11.0. A simulation model was created to represent the configuration of the TERC ACP and assess plant capability and performance dealing with higher CO_2 concentrations than previously investigated. The simulation model provides insight into the relationships between various parameters, in order to predict a variety of scenarios that can be tested on physical plants more efficiently than relying upon experimental iteration alone.

2. DCC model development overview

The simulation model of the TERC ACP has been adapted from the intrinsic Aspen Plus V11.0 configuration file "ENTRL-RK Rate Based MEA Model". This original model has been validated against existing literature and has a user guide accompanying the file [43]. When required, this intrinsic file has been adapted to be more representative of the TERC ACP. The adaptations were based upon a combination of interpreting literature and calibration against existing experimental data. The underlying chemical properties for components in the Aspen Plus database and the source literature upon which the original intrinsic file was based, have been used without modification. The final version of the model is henceforth referred to as the Developed Carbon Capture (DCC) model.

2.1. MEA absorption chemistry and physical properties

Chemistry for the absorption of CO_2 using MEA is shown in Equations (1)–(5), described by Zhang and Chen [44]:

Water Dissociation	$2H_2O \leftrightarrow H_3O^+ + OH^-$	(1)
CO_2 Hydrolysis	$CO_2 + 2H_2O \leftrightarrow HCO_3^- + H_3O^+$	(2)
Bicarbonate Dissociation	$HCO_3^- + H_2O \leftrightarrow MEA + H_3O^+$	(3)
Carbamate Hydrolysis	$MEACOO^- + H_2O \leftrightarrow MEA + HCO_3^-$	(4)
MEA Protonation	$MEAH^+ + H_2O \leftrightarrow MEA + HCO_3^-$	(5)
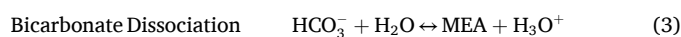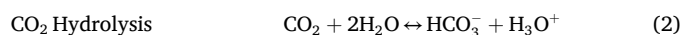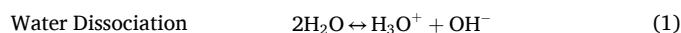
The formations of bicarbonate and carbamate are kinetically limited, in Aspen Plus these have to be represented as twinned competing forward and reverse kinetic reactions. Equations (6) and (7) represent bicarbonate formation, whereas Equations (8) and (9) represent

Table 1
Typical compositions of iron and steel industry process emissions.

Component	Blast Furnace Gas (Average) mol%	Coke Oven Gas (Average) mol%	Blast Furnace + Coke Oven Gas mol%	Basic Oxygen Steelmaking Gas mol%
Carbon Dioxide	24.0	2.0	17.0	15.0
Carbon Monoxide	23.5	5.5	17.5	68.0
Hydrogen	3.5	65.0	24.0	1.0
Methane	–	23.5	8.0	–
Nitrogen	49.0	1	32.5	15.5
Oxygen	–	–	–	0.5

carbamate formation [44]:

$$OH^- + CO_2 \rightarrow HCO_3^- \tag{6}$$

$$HCO_3 \rightarrow OH^- + CO_2 \tag{7}$$

$$MEA + CO_2 + H_2O \rightarrow MEACOO^- + H_3O^+ \tag{8}$$

$$MEACOO^- + H_3O^+ \rightarrow MEA + CO_2 + H_2O \tag{9}$$
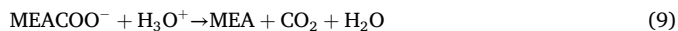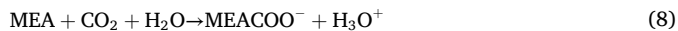
The required reaction kinetics and rate expressions for Equations (6)–(9) are described by Zhang and Chen [44], calculated from the work presented by Hikita et al. [45] and Pinsent et al. [46].

The thermodynamic model adopted for the process simulation uses an electrolyte non-random two-liquid (e-NRTL) activity coefficient model to account for liquid phase nonideality [47], and a perturbed-chain statistical associating fluid theory (PC-SAFT) equation of state (EOS) to account for vapour phase properties [48,49].

Transport property models are required for rate-based process models to calculate the correlations of variables that describe phenomena such as heat transfer, mass transfer, interfacial areas, liquid holdup, pressure drop etc. [50]. Table 2 summarises the models used in Aspen Plus for the calculations in this work.

2.2. The Aspen plus Radfrac™ model

The work conducted by Madeddu et al. [51] has informed the representation of the columns with regards to the underlying properties governing their operation. The RadFrac™model was selected for the absorbing and stripping columns ("absorber" and "stripper" columns) to describe correctly the non-ideal thermodynamics and the chemical reactions, in addition to the interphase transfer, component transport in the different phases and the fluid dynamics. The "Rate-Based Mode" has been selected for the RadFrac™ model because it included limitations to mass transfer due to the presence of chemical reactions, based on Lewis and Whitman's two-film theory [52]. The two-film theory partitions the gas phase and liquid phase, which are separated by the interface, into bulk and film zones. The driving force permits transfer of a gaseous species to occur from the bulk gas, into the gas film, across the interface into the liquid film, then into the bulk liquid. Additional parameters must be specified to fully describe the absorber and stripper columns, including: bulk fluid modelling, film modelling and the number of column stages. Madeddu et al. provides a detailed insight into the options available for each of these choices [51]. A summary of the final key design parameters used in this work is presented in Table 3.

3. The TERC ACP and DCC model validation

3.1. The TERC ACP process description

The Aspen Plus flowsheet of the TERC ACP is presented in Fig. 1, with a process description below it.

Flue gas is blown into the bottom of the absorbing column by a fan from either a synthetic gas mixing skid or from the flue gas manifold that collects gases from combustion and thermo-chemical process plant

Table 2
Physical property methods and models used in the simulation.

Parameter	Liquid	Gas
Density	Clarke Density Model	PC-SAFT EOS Model
Viscosity	Jones-Dole Electrolyte Correction Model	Chapman-Enskog Wilke-Lee Model
Surface Tension	Onsager-Samaras Model	–
Thermal Conductivity	Riedel Electrolyte Correction Model	Stiel-Thodos Model
Binary Diffusivity	Nernst-Hartley Model	Chapman-Enskog Wilke-Lee Model

Table 3
Summary of key design parameters used in the simulation.

Parameter	ACP Model Basis	References
Modelling Approach	Rate-Based Approach	[52]
Number of Theoretical Stages	100	[51]
Flow Model	Mixed	[50,53]
Film Resistance Options	Liquid Phase: "Discretize film" Vapour Phase: "Consider film"	[51]
Liquid Film Discretisation	Discretisation Points = 5 Discretisation Ratio = 10	[51,54]
Reaction Condition Factor	0.9	[50]
Mass Transfer Coefficient Model	Onda-68	[55]
Heat Transfer Coefficient Model	Chilton and Colburn	[56]
Interfacial Area Model	Onda-68 Interfacial Area Tuning Factor = 1.2	[57]
Fractional Liquid Hold-Up Model	Stichlmair89	[58]
Flooding Method	Wallis	[59]

exhausts. The flue gas flows upwards through the structured packing of the column, where it contacts "lean" solvent flowing in a counter current direction. The solvent reacts with the CO_2 in the flue gas, capturing it and becoming "rich", that is, laden with the CO_2. The remaining flue gas leaves the top of the absorber to pass through a two-stage water wash system, to recover any residual solvent. The rich solvent is pumped through a plate heat exchanger to be preheated, before entering the top of the stripper column. The rich solvent flows down the stripper column into the reboiler and heats up, where it releases the bonded CO_2 through the reversible endothermic reaction. The reboiler is supplied with pressurised hot water to provide heat. The CO_2 leaves the top of the stripper and passes through a cooler and then a reflux drum to recover any vapourised water or solvent, which drains back into the stripper. The separated CO_2 stream leaves the top of the reflux drum. The remaining hot solvent, now "lean" due to having less entrained CO_2, leaves the bottom of the reboiler and is pumped back through the plate heat exchanger to preheat the incoming rich solvent. The warm lean solvent passes through a cooler to achieve a temperature set point, before re-entering the top of the absorber to begin a new cycle. The process operates as a closed loop, replenishing minor losses of water and solvent.

The main technical specifications of the TERC ACP are summarised in Table 4. The relevant chemistry, kinetics, thermodynamics, transport properties and RadFrac™ model properties presented in Section 2 describe the absorption and desorption taking place. Operating ranges for key parameters of the plant are presented in Table 5.

3.2. Model convergence logic

The DCC model contains two independent design specifications in order to achieve model convergence.

The first design specification achieves a target capture efficiency for the system. Capture efficiency is calculated through the mass flow difference of CO_2 between the incoming and exiting flue gas around the absorber, after contact with the lean solvent stream. If the specified capture efficiency is not obtained, the model iterates the CO_2 loading of the lean solvent stream to change the solvent capacity, defined as the difference between the rich and lean solvent CO_2 loadings for a given case, allowing for more or less CO_2 capture to take place until the desired target is achieved.

The second design specification balances the CO_2 loading of the hot lean solvent exiting the stripper column with the lean solvent entering the absorber that achieved the target capture efficiency in the first design specification. The model compares the CO_2 loadings of both streams and iterates the reboiler heat duty of the stripper column until the loadings match.
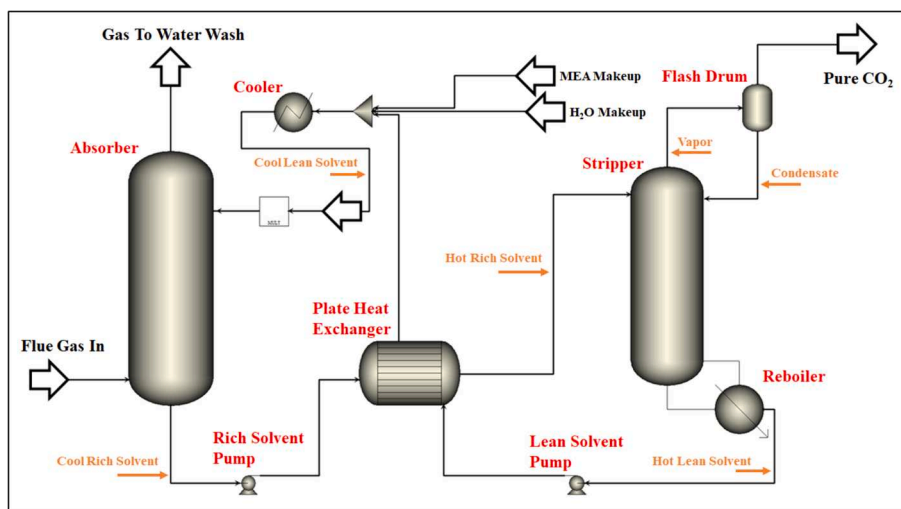
Fig. 1. Process flow diagram of the TERC ACP Aspen Plus V11.0.

Table 4
Technical specifications of the TERC ACP.

Equipment	Specification
Absorber Column	Two 250 mm diameter columns, providing up to 12 m total height
	Packing: 4 x 3 m packed beds of Flexipac 350X structured packing
	12 Resistance Temperature Detectors in each absorber column for temperature monitoring
Stripper Column	Single column of 300 mm diameter with 8 m total height
	Packing: Metal IMPT25 random packing
	9 Resistance Temperature Detectors for temperature monitoring
Heat Exchanger	Plate heat exchanger with maximum heat duty up to 43 kW
Reboiler	Pressurised hot water heated with a 72 kW reboiler

Table 5
Parameter operating ranges of the TERC ACP.

Parameter	Operational Range
Solvent Mass Flow Rate (CO_2 Free Basis)	300 – 1200 kg/h
Flue Gas Volumetric Flow Rate	130 – 210 Nm^3/h
Stripper Column Pressure	1.0 – 2.0 bara

3.3. Model validation

3.3.1. PACT ACP validation

The DCC model was validated against existing ACP data, beginning with a previous study by Akram et al. [36]. The modelled ACP was originally housed at the Pilot-scale Advanced Capture Technology (PACT) facilities at the UK Carbon Capture and Storage Research Centre

(UKCCSRC) and had a different structural configuration for the absorber column: 8 m of height and a 0.3 m diameter packed with IMTP25 random packing. The stripper column, reboiler and cross-heat exchanger are unchanged from those specified in Table 4. The structural configuration of the plant is a significant consideration in optimising different cases because different column diameters or heights will affect performance [36], alongside achieving the balance between flow, mass transport and energy factors for a given plant configuration.

The DCC model simulated the PACT configuration and achieved convergence for all reported cases. The model predictions were evaluated against the reported experimental data. For the modelled flue gas, trace compounds and elements were omitted, with the flue gas consisting of carbon dioxide, water, oxygen and nitrogen. During these experiments, a capture efficiency of approximately 90 % was achieved for every CO_2 concentration by varying the solvent flow rate. The SRD of each CO_2 concentration case is presented in Fig. 2, along with the corresponding CO_2 loadings data.

The SRD predictions from the DCC model are in good agreement with the experimental results, with a mean absolute percentage error (MAPE) of 8.1 %. It is noted in Fig. 2A that the difference in SRD between the model predictions and experimental results reduced with increasing CO_2 concentration, which increases confidence of the model for extrapolations to higher CO_2 concentrations beyond the tested range. Akram et al. [36] discussed the impact that the solvent concentration had on the SRD results, noting that the MEA concentrations of the 6.6 and 8.3 mol% CO_2 cases were lower than expected. This was most likely the result of water transfer from the wash column to the absorber to compensate for evaporative losses, which dilutes the solvent concentration and removes
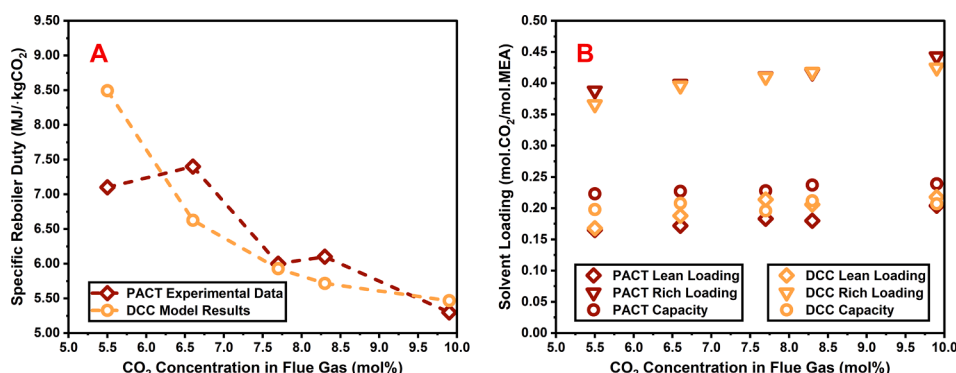
Fig. 2. Specific reboiler duty against flue gas CO_2 concentration for the PACT ACP (A), with corresponding CO_2 loadings data (B).

energy from the system. This transfer of cold water requires energy to achieve the process temperature and increases the overall regeneration energy required in the diluted solvent, due to the higher fraction of water and consequent higher specific heat capacity. The water transfer is not reflected in the DCC model, leading to the lower predicted SRD values for these two cases.

The 5.5 mol% CO_2 case has a larger difference of SRD from the experimental value. Akram et al. [36] established that a solvent flow of 400 kg/hr is the minimum possible for this column size and packing before channelling occurs. The model is over predicting SRD at low solvent flow rates and fails to converge at solvent flows significantly below 400 kg/hr, because of the increasing proportion of water vapor evolved in the reboiler, however this limiting case is not representative of typical operating conditions and the SRD results are valid for the range of cases modelled.

Fig. 2B presents the solvent loadings for the model predictions and experimental data, with the corresponding solvent capacities. The stoichiometry of the reaction between MEA and CO_2 shows that 2 mol of MEA react with 1 mol of CO_2, giving a theoretical maximum CO_2 loading of 0.5 mol·CO_2/mol·MEA, however it is possible to observe CO_2 loadings higher than this [60,61]. The DCC model represented the PACT rich CO_2 loadings well, with a MAPE of 2.2 %. The rich loadings increased with CO_2 concentration, illustrating that the solvent is not fully saturated with CO_2 while still achieving the target capture efficiency. The corresponding lean CO_2 loadings also increased with CO_2 concentration but had a higher MAPE of 9.9 %. This discrepancy is accounted for by the convergence logic of the DCC model, where the lean loading is adjusted iteratively until the target capture efficiency is achieved. It is noted that the DCC model slightly over predicts the lean CO_2 loading, leading to a smaller solvent capacity than in the reported PACT data. This over-prediction is small, with good SRD agreement for the cases, therefore we can be confident in the DCC model's CO_2 loading predictions.

Predicted temperature profiles of the absorber and stripper columns are presented in Fig. 3, which can be compared with the figures presented by Akram et al. [36] as the exact data was not available for recreation.

The exothermic reaction between MEA and CO_2 creates a temperature bulge within the absorber column, indicative of the highest reaction region. The PACT absorber data presented by Akram et al. [36] infers the bulge is occurring towards the top of the column, suggesting that most of the CO_2 is absorbed where the lean solvent enters the column, offering maximum driving force for mass transfer.

The DCC model evidently presents an idealised version of this process in Fig. 3A, predicting the bulge higher up the absorber than the PACT data, likely a result of the flow model selected in Aspen Plus in which the vapour and liquid phases are well mixed throughout the absorber, and the fact that Aspen does not need to represent any sort of liquid distributor at the top of the column. The maximum predicted temperatures are consistent with experimental values but overpredicted

by approximately 3 °C for each idealised case. The validity of the absorber model was demonstrated by the desired capture efficiency and corresponding loadings being consistent with experiments.

CO_2 concentration also has an impact on the temperature profile of the stripper column. Akram et al. recorded the temperature distribution at three points descending the height of the column: at the top, the middle and the bottom [36]. Fig. 3B shows the predictions made by the DCC model for the same temperature distribution points under the same conditions. The DCC model confirms the trend of the PACT data for which the temperature at the top of the column decreases with increasing CO_2 concentration resulting from increased solvent flow rate required for CO_2 capture. The DCC model predicts a gradual decrease in top temperature with increasing CO_2 concentration, whereas the PACT data had greater uncertainty around this trend. The predicted bottom temperature on the column is in excellent agreement with the PACT data, a consequence of the stripper column pressure set at 1.2 bara. The predicted middle temperature is slightly lower than the PACT data, implying that the DCC model has a smoother temperature change descending the height of the column in an idealised representation of the system. The predicted operational performance of the stripper column directly affects the SRD and CO_2 loading of the system, which have already been validated, therefore the overall stripper performance is suitable, giving confidence in the utilisation of the DCC model for predicting operational parameters.

3.3.2. TERC ACP validation

The DCC model subsequently had the absorber updated to that of the TERC configuration and was validated against preliminary data obtained from the TERC ACP. Since the absorber packing material Flexipac 350X is not available in the Aspen Plus V11 database, Flexipac 1X, which has the closest dimensions, was selected instead. A gas flow of 200 Nm^3/h with a CO_2 concentration of 5 mol% was treated with 300 kg/h of solvent with a MEA concentration of 40 wt%. The stripper pressure was fixed at 1.5 bara and the reboiler duty was varied to give different steady state capture efficiencies. Lean solvent and flue gas temperatures were both fixed at 40 °C. Absorber and stripper column temperature data was unavailable for this preliminary test, but the performance may be inferred from the experimental SRD and chemistry data, alongside the previous validation against the PACT ACP. The SRD for each capture efficiency is presented in Fig. 4, along with CO_2 loadings data for one of the cases.

The SRD predictions from the DCC model represent the experimental results well, with a mean absolute percentage error (MAPE) of 1.8 %. The predicted CO_2 loadings for the TERC ACP corroborated the trend noted for the PACT ACP. The predicted rich loading agrees with the TERC data sample and the lean loading is slightly over-predicted, leading to a lower reported solvent capacity. The absorber column change between PACT and TERC has negligible impact on CO_2 loading predictions because the capture efficiency is imposed as described in
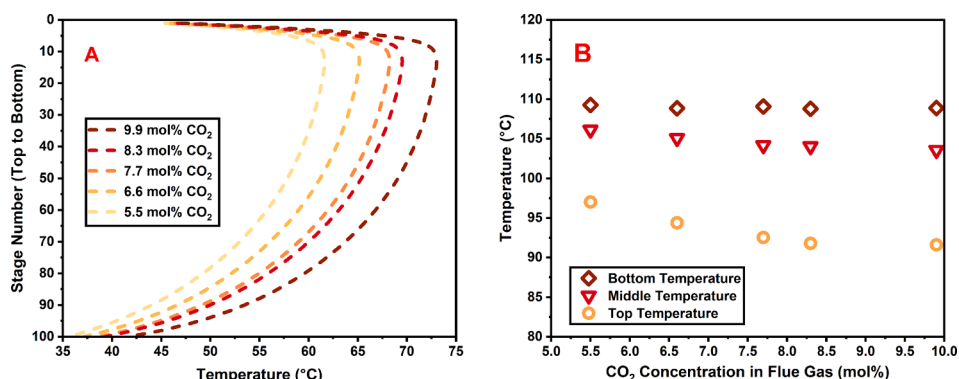
Fig. 3. Absorber temperature profiles with different flue gas CO_2 concentration cases for the PACT ACP (A), with corresponding stripper temperature monitoring (B).
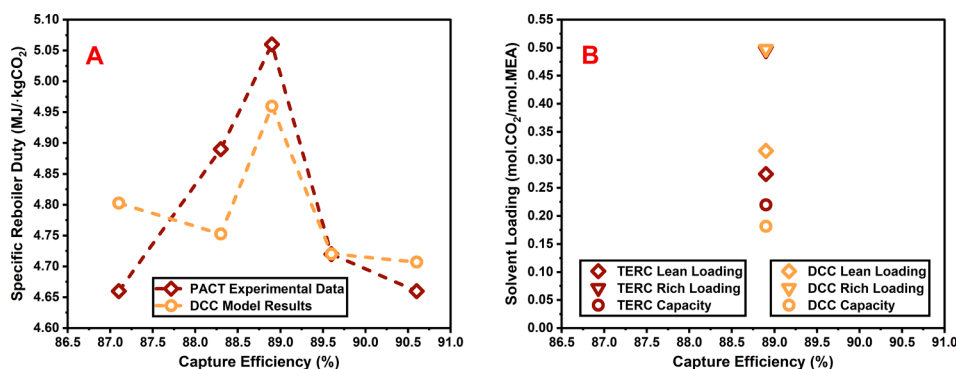
Fig. 4. Specific reboiler duty against capture efficiency for preliminary TERC ACP cases (A), with corresponding CO_2 loadings data for 88.9% capture efficiency (B).

Section 3.2.

The SRD predictions for the TERC ACP are evidently lower than that of the PACT validation, agreeing with the assertion made by Akram et al. that having a taller absorber with additional packing will reduce SRD for the system [36]. As the DCC model gave an acceptable performance against the PACT absorber temperature profiles, we can be confident that the DCC model produces a similarly acceptable performance for TERC absorber temperature profiles through correct representation of the height, diameter and packing of the TERC absorber in Aspen Plus.

The absorber diameter was fixed at 300 mm for continuity of modelling conditions between PACT and TERC cases, with the sensitivity of parameters to changes in column diameter evaluated. Comparison of operating cases demonstrated a maximum increase of 1.7 % in specific reboiler duty (SRD) was predicted, which can be neglected.

The stripper column remains unchanged between PACT and TERC structural configurations. As such, the same conclusions as those seen for the PACT validation are applicable for the TERC validation. The stripper column regenerates the solvent to the correct lean loading with an SRD that is comparable to the preliminary data, confirming the DCC model's robustness with handling a different MEA concentration and stripper column pressure.

With the validation of the DCC model complete, the model has been used to investigate different parameters across a range of flue gas concentrations up to 25 mol% and include: gas volumetric flow rate, solvent mass flow rate, L/G ratios (mass flow of liquid solvent on a CO_2 free basis against the total mass flow of flue gas), column temperature profiles, stripping column pressure, capture efficiency, cross-heat exchanger capacity and SRD. This work identifies trends between these parameters to inform operating regimes when treating flue gases of higher CO_2 concentration that are representative of the iron and steel industry and other foundation industries.

4. Results

4.1. Specific reboiler duty Comparison: 90 % capture efficiency

A comparison of SRD at a range of solvent flow rates and CO_2 concentrations is presented in Fig. 5 for two representative gas flow rates, 130 and 210 Nm^3/h. The capture efficiency achieved was 90 %, achieved when the DCC model converged according to the design specifications outlined in Section 3.2.

For both gas flow rates, concentration of CO_2 ranged from 10 to 25 mol%, increasing in 5 % increments. The water content of the flue gas was kept constant at 3.2 mol% (the average from the PACT validation), with the remaining gas comprising oxygen and nitrogen ratios of air, which is the most likely composition of gases in an experimental campaign. This simplifies the modelling, as only CO_2 can react with the MEA in the DCC model. The range of liquid flow rates from 300 to 1200 kg/h on the x axis is representative of the TERC ACP's capabilities and does not include the mass of CO_2 from the lean loading at steady state conditions. The concentration of the MEA in the solvent was fixed at 35 wt% in every case, on a CO_2 free basis. The temperatures of the lean solvent stream and flue gas stream were fixed at 40 °C. The stripper pressure was kept constant at 1.2 bara. The cross-heat exchanger was set to minimise the approach temperature between the hot rich and hot lean solvent flows in every case, up to the maximum heat duty of 43 kW.

The model predicted that an optimal solvent flow rate, and therefore L/G ratio, occurred for all combinations of volumetric gas flows and CO_2 concentrations, represented as the minimum value of SRD in Fig. 5. The optimal L/G ratio represented a balance between: lean and rich CO_2 loadings for given solvent flow rates achieving the desired capture efficiency and the heat demand of the stripper reboiler. The heat demand encompasses the sensible heat; the heat of vapourisation and the heat of reaction for the system. The heat demand is affected by the stripper pressure and effectiveness of heat integration in the system.

One hypothesis tested using the predictions was that increasing the
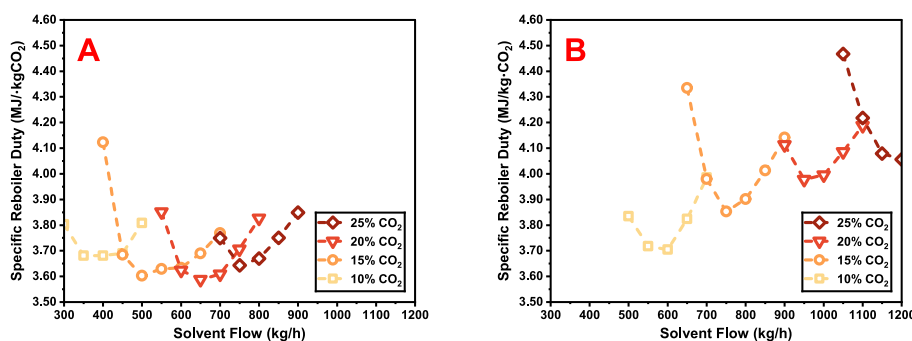
Fig. 5. Specific reboiler duty against solvent flow rate for gas flow rates of 130 Nm^3/h (A) and 210 Nm^3/h (B) for a range of CO_2 concentrations at 90 % capture efficiency.

CO_2 concentration in the flue gas leads to increased SRD at the optimal L/G ratio. The predictions presented in Fig. 5A illustrated that this may not be the case. The minimum SRD when treating a gas flow rate of 130 Nm^3/h was predicted to decrease with increasing CO_2 concentration from 10 to 20 mol% and then increasing for a flue gas with 25 mol% CO_2 concentration.

Conversely, the predictions presented in Fig. 5B appear to support the initial hypothesis, where the SRD demonstrably increased with CO_2 concentration when treating a gas flow of 210 Nm^3/h. This is actually a consequence of exceeding the capacity of the cross-heat exchanger. When the total gas flow rate and CO_2 concentration both increase, a higher solvent flow rate is required to achieve the optimal L/G ratio. Consequently, more heat transfer occurs within the cross-heat exchanger, up to the maximum heat duty of 43 kW.

Beyond this capacity, no additional heat can be transferred into the rich solvent, and the approach temperature in the cross-heat exchanger between the hot rich and hot lean solvent widens with increasing solvent flow rate. The rich solvent stream enters the top of the stripper at a colder temperature, which requires additional heat input from the stripper reboiler for regeneration. This is represented by the incremental differences in predicted SRD presented in Fig. 5B, which relate to the incremental change in the sensible heat of the system resulting from increasing solvent flow rates beyond the capacity of the cross-heat exchanger.

This is important to consider for real life cases because cross-heat exchangers are likely to operate at their maximum capacity when dealing with higher CO_2 concentrations and consequent solvent flow rates. Understanding the impact this will have on the SRD is necessary to ensure that the model data is interpreted correctly.

The predictions presented in Fig. 5A had lower solvent flow rates and all achieved the minimum possible approach temperature with a cross-heat exchanger heat duty below 43 kW, allowing the rich solvent to enter the stripper at the highest possible temperature. This led to the optimal SRD being similar between different CO_2 concentrations at 130 Nm^3/h and indicated that an increasing CO_2 concentration of a flue gas does not necessarily increase the SRD, which is a function of total gas and solvent flow rates and cross-heat exchanger capacity.

It was evident that when accounting for the limitation of the cross-heat exchanger, increased total gas flow rate led to an increase in SRD for the same CO_2 concentration. This relationship was attributed to the higher solvent flow demanded to clean the higher gas flow, which consequently includes a higher flow of water that must be heated and vapourised in the regeneration step, incurring a higher reboiler duty.

A significant trend was identified when comparing the L/G ratios of the data presented across Fig. 5, where it was evident that there was little difference between identified optimal L/G ratios for the same CO_2 concentrations at different gas flow rates, irrespective of the actual SRD and the cross-heat exchanger impact. This allowed simplification of the data so that only the concentration of CO_2 needed to be considered to be able to define initial conditions for plant operation, to achieve a target capture efficiency of 90 %. This trend became apparent due to the constrained nature of the modelled flue gas composition.

For real life cases the flue gas composition may fluctuate, which changes the mass flow rate of the flue gas, making the L/G ratio less useful for predictions. The solvent/CO_2 ratio is an extension of the L/G ratio that isolates the CO_2 of the flue gas flow rate for comparison, defined as the mass flow rate of solvent on a CO_2 free solvent basis against the mass flow rate of CO_2 in the flue gas. It allows for the correct selection of solvent flow rate irrespective of the flue gas composition, as long as the CO_2 concentration in the flue gas is known. The optimal L/G ratios and solvent/CO_2 ratios predicted for gases having CO_2 concentration between 10 and 25 mol% achieving 90 % capture efficiency are presented in Table 6.

It was evident that the predicted optimal L/G ratio for a given CO_2 concentration is constant between the two gas flow rates of 130 and 210 Nm^3/h in the values presented in Table 6, an attribute also shared by the

Table 6

Optimal L/G and solvent/CO_2 ratios for different CO_2 concentrations for 130 Nm^3/h and 210 Nm^3/h gas flow rates with 90 % capture efficiency, with solvent concentration of 35 wt% MEA.

CO_2 Concentration mol%	130 Nm^3/h		210 Nm^3/h	
	L/G Ratio	Solvent/CO_2 Ratio	L/G Ratio	Solvent/CO_2 Ratio
10	2.5	17.1	2.5	17.1
15	3.2	14.9	3.2	14.9
20	3.9	14.0	3.9	14.0
25	4.6	13.5	4.6	13.5

solvent/CO_2 ratio. The optimal L/G ratio demonstrated a linear increase with CO_2 concentration, illustrated by the values predicted for CO_2 concentrations 10 to 25 mol%, for which the optimal L/G ratio increased by approximately 0.7 for each 5 % increase of CO_2 concentration. This trend can be used for predicting approximate optimal L/G ratios to achieve 90 % capture efficiency from any CO_2 concentration for gas flow rates between 130 and 210 Nm^3/h and potentially beyond this range when used with caution.

The solvent/CO_2 ratios decrease with respect to increasing L/G ratio and CO_2 concentration. This is evidently not a perfect linear relationship when assessed by itself and instead relates to the CO_2 loadings data for each optimal L/G ratio, presented in Table 7.

The lean and rich CO_2 loadings data is presented for both 130 and 210 Nm^3/h gas flow rates, along with the calculated solvent capacity. It can be observed that the lean loadings decrease from approximately 0.29 to 0.25 mol·CO_2/mol·MEA as the CO_2 concentration increases from 10 to 25 mol%, whereas the rich loadings remain just above 0.5 mol·CO_2/mol·MEA, indicative that maximum loading has taken place. The predicted solvent capacity increases with CO_2 concentration as a direct result of the increased amount of CO_2 needing to be captured.

The solvent capacity was evidently independent of the total gas flow for a given CO_2 concentration. Crucially, the percentage difference in solvent capacities with increasing CO_2 concentration closely matches the percentage difference in solvent/CO_2 ratios from Table 6, showing they are correlated. These findings are presented in Table 8.

It is evident that the solvent/CO_2 ratio informs the solvent capacity for achieving 90 % capture efficiency across the range of flue gas CO_2 concentrations, where a lower solvent/CO_2 ratio leads to a larger solvent capacity, demonstrating an inverse relationship. As the solvent/CO_2 ratio is related to the L/G ratio (for the flue gas composition described), it can be inferred that the L/G ratio also informs the solvent capacity. Consequently, the linear trend of the L/G ratio can be used for predictions of conditions achieving 90 % capture efficiency across the range of flue gas CO_2 concentrations, and potentially beyond this range. For alternative flue gas compositions with known CO_2 concentrations the solvent/CO_2 ratio may be used for predictions instead because the mass of the flue gas will fluctuate. Predictions using either method can be verified with CO_2 loadings data.

We can conclude that the optimal solvent/CO_2 ratio and solvent

Table 7

CO_2 loadings data for different CO_2 concentrations for 130 Nm^3/h and 210 Nm^3/h gas flow rates with 90 % capture efficiency, with solvent concentration of 35 wt% MEA.

CO_2 Concentration mol%	Lean Loading mol·CO_2/ mol·MEA		Rich Loading mol·CO_2/ mol·MEA		Solvent Capacity mol·CO_2/ mol·MEA	
	130 Nm^3/h	210 Nm^3/h	130 Nm^3/h	210 Nm^3/h	130 Nm^3/h	210 Nm^3/h
10	0.294	0.291	0.505	0.503	0.210	0.211
15	0.271	0.266	0.510	0.506	0.239	0.240
20	0.259	0.254	0.514	0.510	0.256	0.256
25	0.252	0.247	0.517	0.512	0.265	0.265

Table 8

Comparison of percentage differences between solvent capacity and solvent/CO$_2$ ratio with respect to increasing flue gas CO$_2$ concentration, with a solvent concentration of 35 wt% MEA.

CO$_2$ Concentration mol%	Solvent Capacity		CO$_2$ Concentration mol%	Solvent/CO$_2$ Ratio	
	Value mol·CO$_2$/mol·MEA	Increasing % Difference		Value	Increasing % Difference
10	0.210	–	25	13.5	–
15	0.240	12.5	20	14.0	3.6
20	0.256	6.3	15	14.9	6.0
25	0.265	3.4	10	17.1	12.9

capacity, therefore optimal L/G ratio, is independent of gas flow rate and is purely a function of capture efficiency and flue gas CO$_2$ concentration

4.2. Specific reboiler duty Comparison: 95 % capture efficiency

A comparison of SRD at a range of solvent flow rates and CO$_2$ concentrations is presented in Fig. 6 for the two gas flow rates considered, 130 and 210 Nm^3/h, achieving 95 % capture efficiency across the same conditions used for modelling 90 % capture efficiency in Fig. 5. The UK Environment Agency considers 95 % capture efficiency [62] to be the standard attainable for new capture plants to achieve net zero by 2050, moving away from the previous industry target of 90 % capture. The increase in SRD associated with the change from 90 % to 95 % capture efficiency was considered an acceptable energy burden, even as it became increasingly difficult to capture CO$_2$ above 90 % capture efficiency for all conditions modelled.

When comparing Fig. 6 to Fig. 5, the 95 % capture efficiency cases always had a small increase in the SRD over their 90 % capture efficiency counterparts at the minimum L/G ratios. The increase in SRDs ranged from 0.44 % to 1.67 % for 10 to 25 mol% CO$_2$, respectively, when the capture efficiency increased from 90 % to 95 % for a gas flow rate of 130 Nm^3/h. Similarly, the increase in SRDs ranged from 0.57 % to 1.89 % for 10 to 25 mol% CO$_2$, respectively, when the capture efficiency increased from 90 % to 95 % for a gas flow rate of 210 Nm^3/h.

The optimal L/G ratios and solvent/CO$_2$ ratios predicted for gases having CO$_2$ concentration between 10 and 25 mol% achieving 95 % capture efficiency are presented in Table 9.

It is clear that the trends identified for 90 % capture efficiency were still valid, where the predicted optimal L/G ratio and its associated solvent/CO$_2$ ratio is independent of gas flow rate for different flue gas CO$_2$ concentrations achieving 95 % capture efficiency. The CO$_2$ loadings data for 95 % capture efficiency cases presented in Table 10 are assessed and compared against the solvent/CO$_2$ ratios in Table 9.

Examination of the CO$_2$ loadings data and solvent/CO$_2$ ratios for 95 % capture efficiency emphasised the observation of an inverse relationship between these parameters documented in Table 8. This reinforces the findings of Section 4.1, illustrating how the solvent/CO$_2$

Table 9

Optimal L/G and solvent/CO$_2$ ratios for different CO$_2$ concentrations for 130 Nm3/h and 210 Nm3/h gas flow rates with 95 % capture efficiency, with solvent concentration of 35 wt% MEA.

CO$_2$ Concentration mol%	130 Nm^3/h		210 Nm^3/h	
	L/G Ratio	Solvent/CO$_2$ Ratio	L/G Ratio	Solvent/CO$_2$ Ratio
10	2.5	17.1	2.5	17.1
15	3.2	14.9	3.2	14.9
20	4.0	14.3	4.0	14.3
25	4.9	14.4	4.9	14.4

Table 10

CO$_2$ loadings data for different CO$_2$ concentrations for 130 Nm^3/h and 210 Nm^3/h gas flow rates with 95 % capture efficiency, with solvent concentration of 35 wt% MEA.

CO$_2$ Concentration mol%	Lean Loading mol·CO$_2$/mol·MEA		Rich Loading mol·CO$_2$/mol·MEA		Solvent Capacity mol·CO$_2$/mol·MEA	
	130 Nm^3/h	210 Nm^3/h	130 Nm^3/h	210 Nm^3/h	130 Nm^3/h	210 Nm^3/h
10	0.281	0.278	0.503	0.500	0.222	0.221
15	0.257	0.252	0.509	0.505	0.253	0.253
20	0.250	0.245	0.513	0.508	0.263	0.263
25	0.252	0.247	0.514	0.509	0.262	0.262

ratio, therefore L/G ratio, informs the solvent capacity. Consequently, the conclusion of optimal L/G ratio being independent of gas flow rate and purely a function of capture efficiency and flue gas CO$_2$ concentration is strengthened.

While the rich CO$_2$ loadings are comparable between 90 % and 95 % capture efficiency, it is evident that lower lean loadings are generally required to achieve the higher capture efficiency, from 0.28 to 0.25 mol·CO$_2$/mol·MEA, leading to a slightly larger solvent capacity. The exception to this is the 25 mol% CO$_2$ concentration case, which notably required a slightly higher L/G ratio when achieving 95 % capture efficiency over 90 %. This implies that a minimum lean loading of
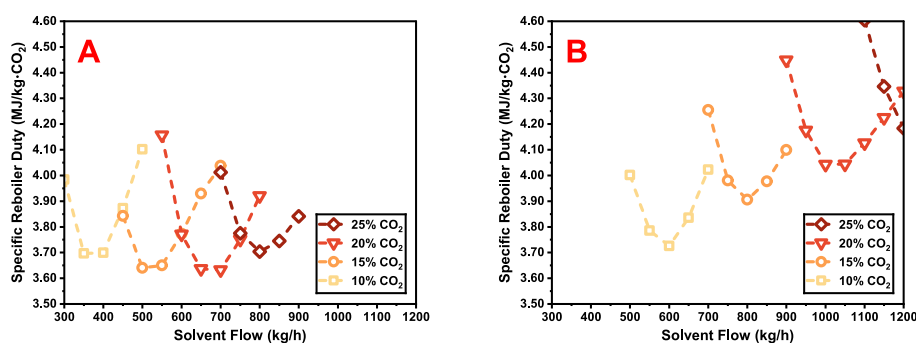
Fig. 6. Specific reboiler duty against solvent flow rate for gas flow rates of 130 Nm3/h (A) and 210 Nm3/h (B) for a range of CO$_2$ concentrations at 95 % capture efficiency.

approximately 0.25 mol·CO₂/mol·MEA is optimal for minimising the SRD of the system when dealing with higher CO_2 concentrations.

The optimal consolidated L/G and solvent/CO₂ ratios, and solvent capacities are presented in Table 11 for different flue gas CO_2 concentrations at 90 % and 95 % capture efficiency, irrespective of total gas flow rate.

For CO_2 concentrations of 10 and 15 mol%, it was found that the optimal L/G and solvent/CO₂ ratio were consistent across both capture efficiencies but it was evident that the optimal L/G ratios started to diverge at higher CO_2 concentrations of 20 and 25 mol%. This is a result of the heat and mass balance of the system achieving the optimal lean CO_2 loading, approximately 0.25 mol·CO₂/mol·MEA therefore leading to similar solvent capacities. The optimal L/G and solvent/CO₂ ratios for 90 % capture efficiency are always less than or equal to 95 % capture efficiency cases, owing to the 95 % cases needing additional solvent to achieve an optimal SRD.

When using these values for guidance in real life capture cases, the CO_2 concentration of the flue gas during operation should be confirmed first, then the desired capture efficiency should be determined, which subsequently informs the selection of L/G or solvent/CO₂ ratio when using 35 wt% MEA solvent. Assessment of CO_2 loading data will describe the system and verify the solvent capacity predictions, ultimately confirming the capture efficiency.

Although the values presented in Table 11 are useful for initial estimates when dealing with gases of different CO_2 concentrations, they do little to explain exactly why these particular L/G ratios are optimal for the given cases. This behaviour can be described through column temperature profiles, investigated in the following section.

4.3. Temperature profiles

4.3.1. Absorber profiles

Absorber operation is described as falling into one of three modes: 1) rich pinched, 2) lean pinched, and 3) bulge pinched. As explained by Weiland et al. [63] operational pinches occur in a column when the actual partial pressure of a component in the vapour at a certain stage approaches the equilibrium vapour pressure of the same component on the same stage. As a result, the driving force for mass transfer reduces to zero and no further mass transfer occurs. Rich end pinches occur at low L/G ratios where the low solvent flow rate has an available solvent capacity corresponding to the amount of CO_2 needing to be removed, meaning the solvent can become fully loaded. Lean end pinches occur at high L/G ratios where the high solvent flow rate has an available solvent capacity greatly exceeding the amount of CO_2 needing to be removed, meaning the solvent is not fully loaded. As the L/G ratio of the system shifts between rich and lean pinched operating regimes it passes through a transition region that exhibits behaviour described as bulge pinched. Bulge pinches make the centre region of the absorber excessively hot and lead to inefficient CO_2 absorption, where only the column ends have effective CO_2 removal. Thus, for a bulge pinched absorber column, the rich solvent is not fully loaded, requiring a "leaner" lean solvent to ensure the required solvent capacity is met to achieve the target capture efficiency, achieved by an increase in stripper reboiler duty which directly leads to a higher SRD [64]. Consequently, bulge pinches should always be avoided in operation. Pinch identification and understanding

can aid problem diagnosis and system optimisation, contributing to explaining the relationship between energy and different L/G ratios for a given case. For further reading, Hatcher et al. describe operational pinches for post-combustion CO_2 capture [64], and for CO_2 removal in a liquid natural gas plant [65].

Pinch conditions can only be verified comprehensively through examining composition profiles [63], but temperature profiles provide a good indicator for the operational mode due to the exothermic reactions taking place. Fig. 7 presents absorber temperature profiles of different L/G ratios for two flue gas flows, 130 and 210 Nm³/h respectively, both gas flows containing 20 mol% CO_2 and all L/G ratios achieving 90 % capture efficiency. The concentration of the MEA in the solvent was fixed at 35 wt% in every case, on a CO_2 free basis. The solvent flow rates do not include the mass of CO_2 from the lean loading at steady state conditions. The temperatures of the lean solvent stream and flue gas stream were fixed at 40 °C. The SRD of these cases was presented in Fig. 5.

Fig. 7A presents the temperature profiles for a volumetric gas flow rate of 130 Nm³/h, which covers a range of L/G ratios from 2.50 to 7.50 for solvent flows 400 to 1200 kg/h. The lower L/G ratios clearly exhibited rich pinched behaviour, characterised by the temperature bulge at the top of the absorption column. It was evident that temperature profile began to evolve into a bulge pinch as the solvent flow rate continued to increase, as the principal reaction region moved down to use more of the column.

Fig. 7B presents temperature profiles for the higher gas flow rate of 210 Nm³/h and has a narrower range of L/G ratios from 2.35 to 4.65 presented for solvent flows 600 to 1200 kg/h. All of the L/G ratios in Fig. 7B exhibited rich pinched trends, however the 1200 kg/h trendline beginning to demonstrate flattened profile typical of a bulge pinch, suggesting if the L/G ratio continued to increase above 4.65 the temperature profiles would transition to a bulge pinch similar to Fig. 7A. The optimal L/G ratio for CO_2 concentration of 20 mol% at 90 % capture efficiency is 3.9, identified in Section 4.1, which is the 1000 kg/h trendline in Fig. 7B. A similar trendline would be expected to fall adjacent to the 600 kg/h trendline in Fig. 7A. These trends are directly related to the optimal mode of operation for stripping columns, described in the next section.

4.3.2. Stripper profiles

Stripper temperature profiles enable inferences about the efficiency of the carbon capture and provide insight into how one would optimise the system. Stripping columns exhibit three distinct behaviours, similar to the absorbing columns. The major difference, however, is that all three stripping behaviours can occur within one absorber operational mode. At high L/G ratios the temperature profiles have little variation from the top of the column where the solvent enters until much lower stages are passed, at which point rapid temperature increases happen. This is known as the "baseline" region. Within the baseline region the rising CO_2/water vapour mixture exchanges heat with the incoming rich solvent, cooling to the same temperature as the incoming solvent and condensing the water such that the CO_2 leaves with as little water vapour as possible [66,67].

If excessive amounts of water vapour are generated by the reboiler, it cannot all be condensed within the stripping column, leading to high

Table 11

Optimal L/G ratios and solvent capacities for different CO_2 concentrations for 90% and 95% capture efficiency, with solvent concentration of 35 wt% MEA.

CO₂ Concentration mol%	90 % Capture Efficiency			95 % Capture Efficiency		
	L/G Ratio	Solvent/CO₂ Ratio	Solvent Capacity mol·CO₂/mol·MEA	L/G Ratio	Solvent/CO₂ Ratio	Solvent Capacity mol·CO₂/mol·MEA
10	2.5	17.1	0.210	2.5	17.1	0.222
15	3.2	14.9	0.240	3.2	14.9	0.253
20	3.9	14.0	0.256	4.0	14.3	0.263
25	4.6	13.5	0.265	4.9	14.4	0.262
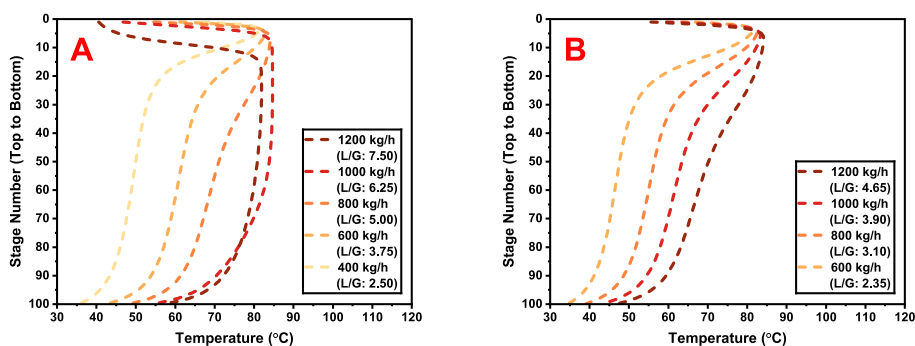
Fig. 7. Absorber temperature profiles with gas flow rates of 130 Nm^3/h (A) and 210 Nm^3/h (B) with a CO_2 concentration of 20 mol%, treated with 35 wt% MEA solvent flow rates to achieve 90 % capture efficiency.

concentrations of water vapour at the top of the column alongside rapid temperature increase of the incoming solvent. Stripper operation with this condition means that energy in the reboiler is wasted because some of the water vapour was not condensed, leading to an exponential increase in SRD [67,68]. Consequently, this is known as the "exponential" region. The transition from the baseline region to the exponential region must pass through an operating regime between these two extremes, with an optimal energy configuration known as the "inflection" point occurring within this transition region. Just like the baseline region, the CO_2 leaves the top of the column with as little water vapour as possible, the difference being that water condensation happens across the whole height of the column in a smooth transition of energy, owing to the solvent flow rate being lower than the baseline region, therefore minimising the energy input. It is recommended to operate as close to the inflection point as possible to minimise the SRD [66–68]. The stripper temperature profiles corresponding to the cases in Fig. 7 are presented in Fig. 8, emphasising the three distinct regions across the range of temperature profiles.

Evidently from Fig. 8A the higher L/G ratios $\geq$ 5.00 have temperature profiles within the baseline region. The increasing L/G ratio across the baseline region related to the temperature profiles transitioning from rich pinched to bulge pinched in Fig. 7A, emphasising that the solvent flow is too high to achieve optimal SRD. The lowest solvent flow rate of 400 kg/h was within the exponential region, created through the surplus water vapour that could not condense. The solvent flow of 600 kg/h gave rise to a temperature profile between these two regions and demonstrated a more uniformly increasing temperature as the fluid descended the column. The predicted optimal L/G ratio was evaluated to be 3.9, whilst the temperature profile for a solvent flow rate of 600 kg/h related to a L/G ratio of 3.75, considered to approximate the inflection point.

Fig. 8B illustrates a smaller range of L/G ratios but still demonstrated the three operating zones described. The lower L/G ratios were in the exponential region, and the highest were in the baseline region, with the

remaining temperature profile, at a L/G ratio of 3.9, following a curve that approximated to the inflection point region. This L/G ratio was predicted to be within the region of optimal SRD and the determined temperature profile validated that claim. It should be noted that all of these operating zones occur in the stripper but Fig. 7B illustrated that these operating behaviours were still considered to have rich pinched temperature profiles in the absorber. It is not valid to claim that specific pinch operating conditions in an absorber relate to a certain operating region in the stripper and both should be assessed to fully understand the capture system.

Crucially, these temperature profiles provide further insight into the SRD graphs presented in Sections 4.1 and 4.2. If one considers the 20 mol% CO_2 trends from Fig. 5, the inflection points from Fig. 8 related to the minimum SRDs. Increasing the solvent flow from the minimums in Fig. 5 increased the SRD and the system transitioned into the baseline region of stripper operation. Decreasing solvent flow from the minimum also increased SRD, as a result of the system transitioning into the exponential region of stripper operation. It is these relationships that aid explanation and understanding of the system affording a more complete understanding of the capture system to be determined from simple energy plots.

4.3.3. Optimal liquid to gas ratio temperature profiles

Having established the different operational modes of absorbing and stripping columns, alongside their role in energy optimisation of the capture system, it is logical to assess the temperature profiles predicted for the optimal L/G ratios identified in Table 11 to establish if they are optimal cases. Fig. 9 presents the absorber temperature profiles for the predicted optimal L/G ratios from Table 11.

Despite the difference in gas flow rate between the two cases, Fig. 9 presents all of the cases exhibiting rich pinch operational behaviour for both capture efficiencies, with adjacent temperature profiles of the same shape for all cases. The temperature difference between plots is a result of the increasing exothermic reaction energy with respect to increasing
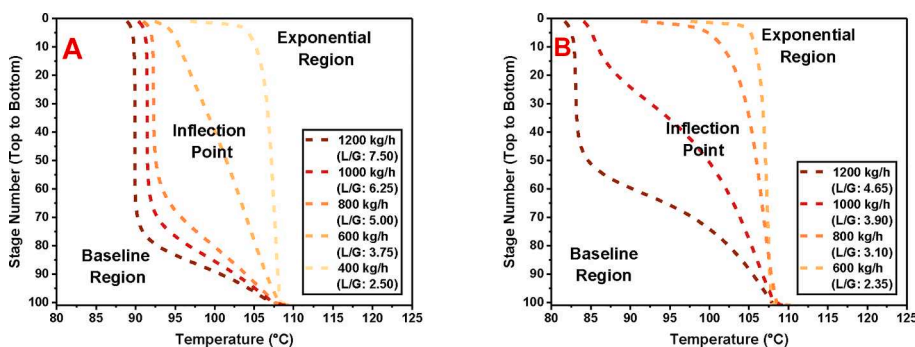
Fig. 8. Stripper temperature profiles with gas flow rates of 130 Nm^3/h (A) and 210 Nm^3/h (B) with a CO_2 concentration of 20 mol%, treated with 35 wt% MEA solvent flow rates to achieve 90 % capture efficiency.
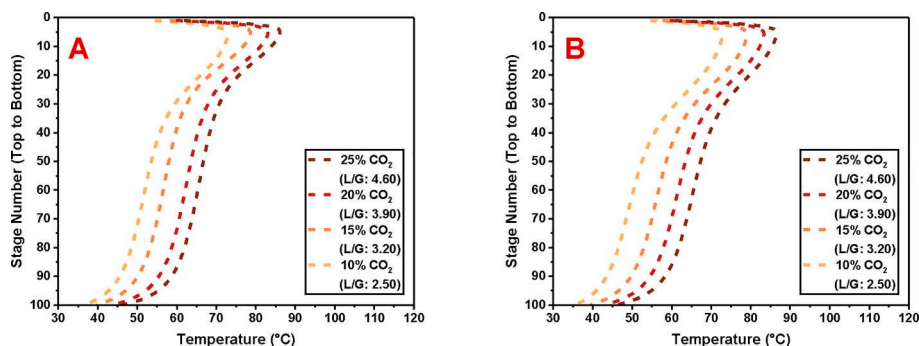
Fig. 9. Absorber temperature profiles with gas flow rates of 130 Nm^3/h (A) and 210 Nm^3/h (B) for a range of CO_2 concentrations at predicted optimal L/G ratios to achieve 90 % capture efficiency.

flue gas CO_2 concentration. The difference in flue gas flow rate has negligible effect on the temperature plots, further illustrating that the optimised L/G ratio is independent of the flue gas flow rate and is purely a function of capture efficiency and CO_2 concentration. This also highlights that the TERC ACP system operates optimally with a rich pinch set up. It has already been shown that lean pinch operation is not usually possible for higher CO_2 concentrations within the operating solvent flow rate range and bulge pinches should always be avoided, so naturally a rich pinch operation should be expected.

For these L/G ratio predictions, it should be expected to see temperature profiles that follow curves similar to the inflection point for the stripper. Fig. 10 presents the corresponding stripper temperature profiles for the cases presented in Fig. 9 for analysis.

Fig. 10 appears to show different behaviours for the proposed optimal L/G ratios, but these can be explained with consideration of the cross-flow heat exchanger. For the 130 Nm^3/h cases in Fig. 10A, the cross-heat exchanger minimised the approach temperature between the hot rich and hot lean solvents, leading to similar temperatures at the top of the stripper column. For the 210 Nm^3/h cases, the heat duty of the cross-heat exchanger had reached a maximum and was unable to heat the higher solvent flow rates sufficiently, where the approach temperature between the hot rich and hot lean solvent widened with increasing solvent flow, contrasting with the 130 Nm^3/h cases. As a result, increasing solvent flow rates led to decreasing temperatures at the top of the stripper column and exhibited a "crossover" temperature profile as the solvent flow begins to be heated upon descending the column. In an ideal scenario, the cross-heat exchanger would have a larger heat capacity to minimise the approach temperature for the hot rich solvent, then the different solvent flow rates would be expected to have similar temperatures at the top of the stripper column. Irrespective of this, Fig. 10B depicts what would happen in a stripping column of a real-life plant that is operating at solvent flows beyond the maximum heat exchanger capacity, the effects of which must be understood to correctly describe the behaviour of the column and aid system optimisation.
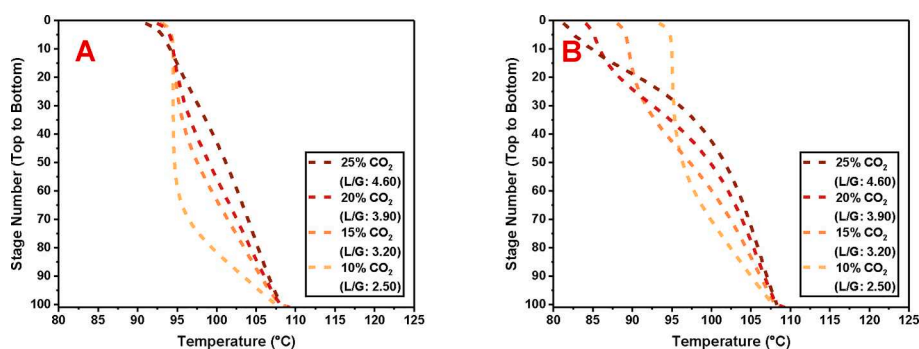
Irrespective of this nuance, the temperature profiles approximate inflection point operation after the first 30 stages of the stripper illustrated in Fig. 10B. The temperature profiles transition to a uniformly distributed temperature increase, as predicted, meaning the predicted L/G ratios were valid optimums. Fig. 10A presents an interesting outlier for 10 mol% CO_2 case, since the temperature profiles of 15 to 25 mol% CO_2 appeared to be operating approximately at the inflection point, confirming the validity of the L/G ratio predictions, this was not the case for 10 mol% CO_2, which appeared to be in the baseline region. Reviewing the SRD versus L/G relationships presented in Fig. 5A it was evident that the minimum SRD was flat over a small range of L/G ratios. The prediction of L/G ratio in that case did not result in a stripper temperature profile at the precise inflection point. This does not necessarily mean, however, that the optimisation is completely wrong. As the minimum SRD spans a narrow range of L/G ratios, this gives some flexibility of operating point for the system and demonstrates that it is possible to achieve very close to the minimum SRD even if the associated L/G ratio does not match operation exactly at the inflection point.

All of the cases thus far were investigated at a constant stripper pressure of 1.2 bara. The stripper pressure can have significant impacts on the energy optimisation of the system, discussed in the following section.

4.4. Stripping column pressure implications

The effect that the stripping column pressure had on the SRD was also considered across different CO_2 capture efficiencies and gas flow rates with different CO_2 concentrations. The stripper pressure affected the bottom temperature and temperature distribution of the column. A higher pressure led to a higher stripper bottom temperature, which affected the efficiency of the endothermic reactions to release the entrained CO_2 from the solvent. It should be possible to determine the optimal L/G ratio and SRD for a given operating scenario of fixed stripping pressure, and then modify the stripping pressure for a second-

Fig. 10. Stripper temperature profiles with gas flow rates of 130 Nm^3/h (A) and 210 Nm^3/h (B) for a range of CO_2 concentrations, at predicted optimal L/G ratios to achieve 90 % capture efficiency.

stage optimisation step in an effort to further reduce the energy demand of the system at that L/G ratio. A range of stripper pressure cases from 1.0 bara to 2.0 bara for different gas flow rates at a CO_2 concentration of 20 mol%, with gas and solvent flow rates at the relevant optimal L/G ratios for a solvent concentration of 35 wt% MEA, are presented in Fig. 11 for 90 % capture efficiency. Fig. 11A shows predictions when the cross-heat exchanger was constrained to a heat duty of 43 kW, and Fig. 11B shows predictions with a minimum approach temperature between the hot rich and the hot lean solvent.

The key observation about the predictions presented in Fig. 11A was that the SRD would be significantly higher than the minimum unless the optimal stripper pressure was identified for a given scenario. The optimal stripper pressure was approximately 1.2 – 1.3 bara at 90 % capture efficiency. The overall trends were assessed to be the same when achieving 95 % capture efficiency, with the optimal stripper pressure increasing by approximately 0.1 bar to 1.3 – 1.4 bara. Evidently, operating with marginally higher stripper pressures may be advantageous for reducing SRD at higher capture efficiency. It was evident that the observed trend of SRD increasing with stripper pressure was a result of the fixed heat capacity of the cross-heat exchanger. This constrained evaluation can be useful for operation of the TERC ACP and any other real-life cases that may be running at maximum cross-heat exchanger capacity but disguises the actual impact of the stripper pressure. In these cases, as the stripper pressure increases, the bottom temperature increases as a result of how the stripper pressure affects the boiling point of the solvent mixture. Consequently, the hot rich and hot lean approach temperature in the cross-heat exchanger begins to widen, meaning the solvent enters the top of the stripper at similar temperatures for all stripper pressures, requiring increasing SRD to get the solvent to temperature.

These modelled cases were repeated, incorporating a minimum approach temperature between the hot rich and the hot lean solvent for the cross-heat exchanger to get a better understanding of the effect of pressure on SRD without the constrained heat integration, with the results presented in Fig. 11B. Here the impact of the stripper pressure on the SRD of the idealised system is clear: increasing pressure reduces the SRD in every case. This demonstrates that heat integration is vital for minimising SRD, where a cross-heat exchanger with the capacity to achieve the lowest approach temperature between the hot rich and hot lean solvents should be utilised wherever possible.

With the impact of the cross-heat exchanger on SRD with changing pressure understood, the temperature profiles of the stripper column may be assessed for both scenarios: fixed cross-heat exchanger duty and minimised approach temperature, presented in Fig. 12. The selected gas flow rate of 210 Nm^3/h with CO_2 concentration of 20 mol% achieving 90 % capture efficiency is used to investigate the stripper column temperature profiles for a cross-heat exchanger constrained to 43 kW in Fig. 12A, and for a minimum approach temperature between the hot rich and hot lean solvent in Fig. 12B.

The solvent boiling point increases as a function of stripper pressure,

leading to an increase in the temperature of the vapour generated by the reboiler. Consequently, the system begins to transition to baseline operation within the stripper, where the temperature profiles have little variation from the top of the column progressively to the lower stages with increasing pressure. At this point the increasingly hot vapour mixture rapidly condenses leading to a significant temperature increase of the downflowing rich solvent.

As stripper pressures reduce, the solvent boiling point decreases and the system begins to transition to exponential operation, or which an increasing amount of vapour is unable to condense within the stripper column leading to an increasing concentration of water at the top of the column.

The major difference between Fig. 12A and Fig. 12B is the temperature at the top of the stripper column, where Fig. 12A is representative of real life cases with constrained heat integration arising from the cross-heat exchanger capacity, while Fig. 12B represents idealised conditions with maximum heat integration. A stripper pressure of 1.2 bara in Fig. 12A approximates the inflection point of the constrained system, consistent with a minimal SRD noted in Fig. 11A. Fig. 12B exhibits the three distinct stripper column behaviours but the SRD continues to reduce with increasing pressure due to maximum heat integration, making identification of optimal operating conditions less obvious from the stripper temperature profile alone. This implies that the existence of an optimal inflection point is a feature of constrained heat integration, albeit a more realistic representation of a system.

The assessment across different flue gas CO_2 concentrations can be verified using the understanding of how the system is operating for different stripper pressures at a fixed CO_2 concentration. For this, a range of stripper pressure variation cases from 1.0 to 2.0 bara for different CO_2 concentrations at a gas flow rate of 150 Nm^3/h are presented in Fig. 13, with the gas flow rate at its optimal L/G ratio for each respective CO_2 concentration to achieve 90 % capture efficiency. Fig. 13A has the cross-heat exchanger constrained to a heat duty of 43 kW and Fig. 13B employs the minimum approach temperature between the hot rich and hot lean solvent.

Notably, the major trend shown for Fig. 13A is that increasing the CO_2 concentration consistently led to an increase in SRD for any pressure, illustrated by the plots not incurring crossover. The overall trends follow same pattern as the cases in Fig. 11A, corroborating that SRD increasing with stripper pressure was a result of the fixed heat capacity of the cross-heat exchanger. For the TERC ACP, a narrow stripping pressure range of 1.2 to 1.3 bara could be considered optimal for the system, agreeing with the analysis of Fig. 11A, where the stripper operates approximately around the inflection point and minimises the SRD of the system as shown in Fig. 12A. Analysis of Fig. 13B shows decreasing SRD with increasing stripper pressure when the minimum approach temperature is used, in agreement with Fig. 11B.

Optimisation of the stripping column pressure is a multi-objective problem, where the L/G ratio, CO_2 concentration of the gas stream, level of heat integration and desired capture efficiency all influence the
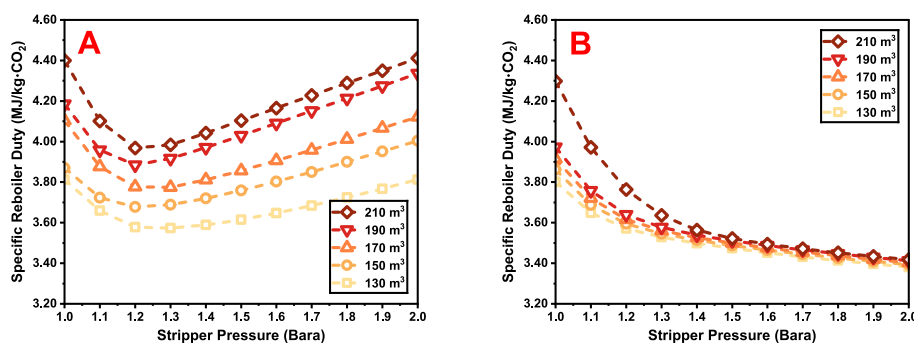
Fig. 11. Specific reboiler duty against stripper pressure for various gas flow rates with a CO_2 concentration of 20 mol%, achieving 90 % capture efficiency at their optimal L/G ratios for cross-heat exchanger duty of 43 kW (A) and minimised hot rich and hot lean solvent approach temperature (B).
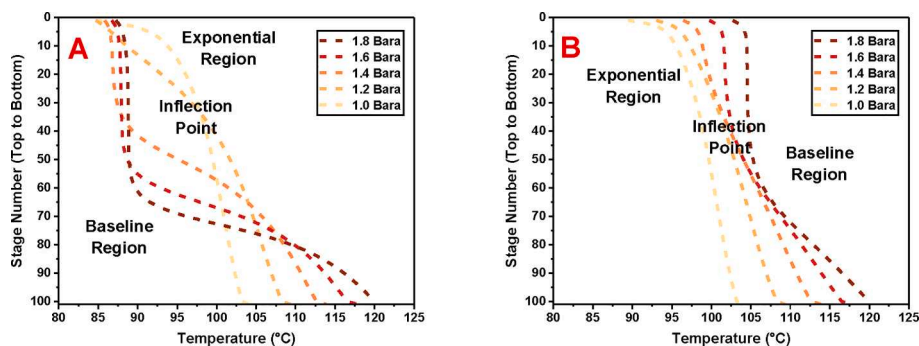
Fig. 12. Stripper temperature profiles with gas flow of 210 Nm^3/h with a CO$_2$ concentration of 20 mol% for a range of stripper pressures achieving 90 % capture efficiency with a cross-heat exchanger duty of 43 kW (A) and minimised hot rich and hot lean solvent approach temperature (B).
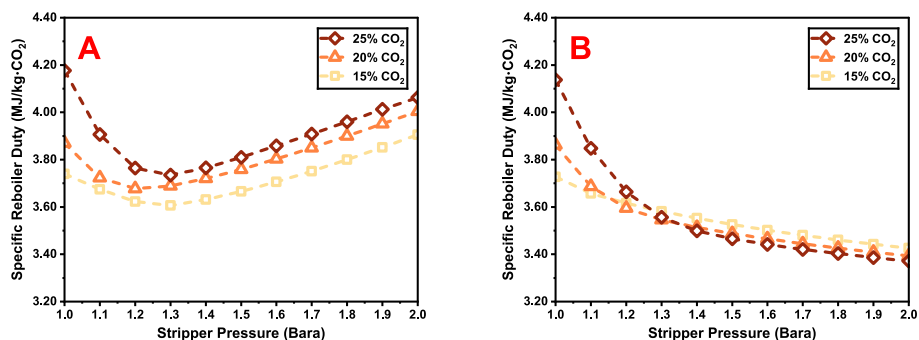
Fig. 13. Specific reboiler duty against stripper pressure for 150 Nm^3/h gas flow rates with a range of CO$_2$ concentrations achieving 90 % capture efficiency with a cross-heat exchanger duty of 43 kW (A) and minimised hot rich and hot lean approach temperature (B).

ideal stripper pressure and must be investigated to maximise the energy efficiency of the system. For systems with very large capacities of cross-heat exchangers, the system simplifies, because the hot rich solvent stream will enter the top of the stripping column at the highest temperature possible. However, for real life cases this will not always be possible, so understanding the impact that the cross-heat exchanger is having on a system is essential.

5. Conclusions

A rate-based model representation of the ACP located at TERC, Sheffield, was developed in Aspen Plus V11.0 to evaluate operational performance and capability for CO$_2$ absorption with MEA dealing with flue gases containing high CO$_2$ concentrations typical of iron and steel making industrial processes.

The validated DCC model successfully predicted a range of ACP capabilities for CO$_2$ concentrations above the upper threshold of testing carried out in previous studies. The predicted data enabled identification of optimal L/G ratios for different cases, defined as minimising the SRD, while inferring trends between different operating parameters, including: volumetric gas flow, CO$_2$ concentration, L/G ratio, capture efficiency, stripper pressure and cross-heat exchanger heat duty.

The following conclusions can be drawn from the results:

- Optimal L/G ratios are independent of gas flow rates and are instead a function of capture efficiency and CO$_2$ concentration. This was apparent through investigation of the solvent loadings required for a target capture efficiency, which had the same solvent capacities at different gas flow rates for a specified CO$_2$ concentration and capture efficiency.
- Optimal L/G ratios of all test cases occurred within a range of 2.5 to 4.6 for 90 % capture efficiency and 2.5 to 4.9 for 95 % capture efficiency across the range of flue gas CO$_2$ concentrations.

- For the optimal L/G ratios of all test cases the associated lean solvent loadings occurred within a range of 0.245 to 0.294 mol·CO$_2$/mol·MEA, and the associated rich solvent loadings occurred within a range of 0.500 to 0.517 mol·CO$_2$/mol·MEA.
- Optimal L/G ratios have a corresponding solvent/CO$_2$ ratio that is closely linked to the solvent capacity, a relationship that is not evident through L/G ratio alone.
- Optimal solvent/CO$_2$ ratios of all test cases occurred within a range of 17.1 to 13.5 for 90 % capture efficiency, and 17.1 to 14.3 for 95 % capture efficiency across the range of flue gas CO$_2$ concentrations.
- For lower flue gas CO$_2$ concentrations of 10 and 15 mol% the predicted optimal L/G and solvent/CO$_2$ ratios are the same for both 90 and 95 % capture efficiency.
- For higher flue gas CO$_2$ concentrations of 20 and 25 mol% the predicted optimal L/G and solvent/CO$_2$ ratios were observed to be slightly higher for 95 % capture efficiency over 90 % capture efficiency. For these cases the lean solvent loading approximated 0.25 mol·CO$_2$/mol·MEA., inferred to be the optimal for the system.
- Optimal L/G ratios may be used for initial predictions in systems with similar flue gas composition to the one described for this work.
- Optimal solvent/CO$_2$ ratios may be used more generally for initial predictions where the flue gas composition differs from this work, as long as the CO$_2$ concentration in the flue gas is known.
- The heat duty of the cross-heat exchanger affected the SRD for gas flow rates of 210 Nm^3/h but did not the predicted CO$_2$ loadings.
- Absorber column temperature profiles should be assessed as an initial starting point to ensure that the mode of operation falls in either a rich pinched or lean pinched scenario, avoiding bulge pinches at all times. When possible, absorber column composition profiles should ultimately be used to identify and assess the status of pinches in the absorber column to aid detailed system optimisation.
- Stripper column temperature profiles should be observed, and adjustments made to ensure that the system operates as close to the

inflection point as possible, thereby achieving a minimum SRD for systems with constrained heat integration. Operating regimes outside of the inflection point for constrained heat systems incur an SRD penalty but may not be the case for idealised heat integration. The baseline region is typically associated with high L/G ratios and the exponential region is associated with low L/G ratios.

- The minimal SRD of a case may appear flat over a range of solvent flow rates. The optimal L/G ratio can be confirmed through assessment of stripper temperature profiles and calibrated to achieve the inflection point.
- The impact of heat duty from the cross-heat exchanger is essential to correctly understand stripper column temperatures. At a minimum approach temperature in an ideal system, the hot rich solvent enters the top of the stripper at the maximum temperature possible and the operating regimes will be evident across different L/G ratios. With constrained heat integration, typical of real plants, the temperature of the hot rich solvent entering the stripper will vary in accordance with the solvent flow rate and the L/G ratio, imposing different stripper temperature profiles.
- The cross-heat exchanger can mask the impact of stripper pressure. In a constrained system there is an optimal stripper pressure associated with the cross-heat exchanger that leads to a minimum SRD. For an ideal system with a minimum approach temperature for the cross-heat exchanger, increasing stripper pressure results in decreasing SRD.
- Optimisation of the stripping column pressure is a multi-objective problem, where the L/G ratio, CO_2 concentration of the gas stream, level of heat integration and desired capture efficiency all influence the ideal stripper pressure. A stripper pressure between 1.2 and 1.4 bara closely approximates operation around the inflection point for the TERC system.

The validated DCC model is a useful tool for future simulation and optimisation work on chemical absorption systems treating flue gases with high CO_2 concentration typical of the iron and steel industry, being able to quickly determine optimal operating conditions for a given case. Future work will involve a comprehensive experimental campaign to provide a comparison between predicted conditions and plant results, thereby enabling calibration of the model and subsequent improvement of the DCC model. The DCC model can represent other plants with alternative structural configurations, with the caveat that model calibration will be required for increased prediction accuracy.

The relationships identified between operational parameters in this work provides invaluable knowledge for real life MEA absorption systems dealing with wide ranges of flue gas CO_2 concentrations. Identified L/G or solvent/CO_2 ratios can provide initial setpoints for solvent flows for a given flue gas, with CO_2 loadings confirming achieved capture efficiency. Observation of column temperature profiles can aid solvent flow calibration to achieve faster optimisation to minimise the SRD of the system.

CRediT authorship contribution statement

Jack Wells: Writing – original draft, Validation, Methodology, Investigation, Formal analysis, Data curation, Conceptualization. **Andy Heeley:** Writing – review & editing. **Muhammad Akram:** Writing – review & editing, Supervision, Investigation, Conceptualization. **Kevin J. Hughes:** Writing – review & editing, Supervision, Methodology, Conceptualization. **Derek B. Ingham:** Writing – review & editing, Supervision. **Mohamed Pourkashanian:** Supervision, Resources, Project administration, Funding acquisition, Conceptualization.

Declaration of competing interest

The authors declare that they have no known competing financial interests or personal relationships that could have appeared to influence the work reported in this paper.

Data availability

Data will be made available on request.

Acknowledgements

References

[1] NASA Earth Science Communications Team. Carbon Dioxide Concentration | NASA Global Climate Change. Climate Change: Vital Signs of the Planet 2023. https://climate.nasa.gov/vital-signs/carbon-dioxide (accessed December 14, 2023).

[2] Lacis AA, Schmidt GA, Rind D, Ruedy RA. Atmospheric CO2: Principal Control Knob Governing Earth's Temperature. Science 2010;330:356–9. https://doi.org/10.1126/science.1190653.

[3] Masson-Delmotte, V., P. Zhai, A. Pirani, S. L. Connors, C. Péan, S. Berger, N. Caud, Y. Chen L, Goldfarb, M. I. Gomis, M. Huang, K. Leitzell, E. Lonnoy, J.B.R. Matthews, T. K. Maycock TW, O. Yelekçi RY and BZ (eds.). Climate Change 2021: The Physical Science Basis. Contribution of Working Group I to the Sixth Assessment Report of the Intergovernmental Panel on Climate Change. Cambridge University; 2021.

[4] UNFCCC. United Nations Framework Convention on Climate Change United Nations. United Nations Framework Convention on Climate Change 1992:1–33.

[5] Grubb M. Kyoto and the Future of International Climate Change Responses: From Here to Where. Int Rev Environ Strateg 2004;5:15–38.

[6] United Nations (UN). The Paris Agreement. 2015.

[7] GOV.UK. UK becomes first major economy to pass net zero emissions law 2019. https://www.gov.uk/government/news/uk-becomes-first-major-economy-to-pass-net-zero-emissions-law (accessed August 25, 2021).

[8] Committee on Climate Change (CCC). The Sixth Carbon Budget: The UK's path to Net Zero. Committee on Climate Change 2020:448.

[9] Swalec C. Guest post: These 553 steel plants are responsible for 9% of global CO2 emissions. Carbon Brief 2021. https://www.carbonbrief.org/guest-post-these-553-steel-plants-are-responsible-for-9-of-global-co2-emissions/ (accessed December 14, 2023).

[10] Global Efficiency Intelligence. Iron and Steel Industry. Global Efficiency Intelligence 2023. https://www.globalefficiencyintel.com/steel-industry (accessed December 14, 2023).

[11] World Steel Association. Steel Statistical Yearbook 2022 2022.

[12] Wiley DE, Ho MT, Bustamante A. Assessment of opportunities for CO2 capture at iron and steel mills: An Australian perspective. Energy Procedia 2011;4:2654–61. https://doi.org/10.1016/j.egypro.2011.02.165.

[13] Huth M, Heilos A. 14 - Fuel flexibility in gas turbine systems: impact on burner design and performance. In: Jansohn P, editor. Modern Gas Turbine Systems, Woodhead Publishing; 2013, p. 635–84. Doi: 10.1533/9780857096067.3.635.

[14] Wallach O. Green Steel: Decarbonising with Hydrogen-Fueled Production. Visual Capitalist 2022. https://www.visualcapitalist.com/sp/green-steel-decarbonising-with-hydrogen-fueled-production/ (accessed December 14, 2023).

[15] H2 green steel. Green Steel production. H2 Green Steel 2022. https://www.h2greensteel.com/articles/green-steel-production (accessed December 14, 2023).

[16] IEA. The Future of Hydrogen – Analysis. IEA 2019. https://www.iea.org/reports/the-future-of-hydrogen (accessed December 14, 2023).

[17] Eh Christina L. M., Tiong Angnes N. T., Kansedo Jibrail, Lim Chun Hsion, How Bing Shen, Ng Wendy Pei Qin. Circular Hydrogen Economy and Its Challenges. Chemical Engineering Transactions 2022;94:1273–8. Doi: 10.3303/CET2294212.

[18] Nakano N, Inada T, Katayama K, Ujisawa Y, Oboso A. Advanced Technologies for Blast Furnace Life Extension 2020.

[19] Vogl V, Olsson O, Nykvist B. Phasing out the blast furnace to meet global climate targets. Joule 2021;5:2646–62. https://doi.org/10.1016/j.joule.2021.09.007.

[20] IRENA. Potential Green Hydrogen Uses In Industry And Related Barriers. Green hydrogen for industry: A guide to policy making, Abu Dhabi: 2022.

[21] IEA. Energy Technology Perspectives 2020 – Analysis. IEA 2020. https://www.iea.org/reports/energy-technology-perspectives-2020 (accessed December 14, 2023).

[22] IEA. Iron and Steel Technology Roadmap – Analysis. IEA 2020. https://www.iea.org/reports/iron-and-steel-technology-roadmap (accessed December 14, 2023).

[23] IEA. Net Zero by 2050 – Analysis. IEA 2021. https://www.iea.org/reports/net-zero-by-2050 (accessed December 14, 2023).

[24] Element Energy. DEEP DECARBONISATION PATHWAYS FOR UK INDUSTRY. Climate Change Committee (CCC) 2020.

[25] Han K, Ahn CK, Lee MS. Performance of an ammonia-based CO2 capture pilot facility in iron and steel industry. Int J Greenhouse Gas Control 2014;27:239–46. https://doi.org/10.1016/j.ijggc.2014.05.014.

[26] Chung W, Roh K, Lee JH. Design and evaluation of CO2 capture plants for the steelmaking industry by means of amine scrubbing and membrane separation. Int J

Greenhouse Gas Control 2018;74:259–70. https://doi.org/10.1016/j. ijggc.2018.05.009.

[27] Cachola C da S, Ciotta M, Azevedo dos Santos A, Peyerl D. Deploying of the carbon capture technologies for CO2 emission mitigation in the industrial sectors. Carbon Capture Science & Technology 2023;7:100102. Doi: 10.1016/j.ccst.2023.100102.

[28] IEA. Iron and Steel CCS Study (Techno-Economics Integrated Steel Mill) 2013. https://ieaghg.org/docs/General_Docs/Reports/2013-04.pdf (accessed December 14, 2023).

[29] Arasto A, Tsupari E, Kärki J, Pisilä E, Sorsamäki L. Post-combustion capture of CO2 at an integrated steel mill – Part I: Technical concept analysis. Int J Greenhouse Gas Control 2013;16:271–7. https://doi.org/10.1016/j.ijggc.2012.08.018.

[30] CO2 Value Europe. CCU Projects Database. CO2 Value Europe 2018. https://data base.co2value.eu/projects/119 (accessed January 29, 2024).

[31] Dreillard M, Broutin P, Briot P, Huard T, Lettat A. Application of the DMXTM CO2 Capture Process in Steel Industry. Energy Procedia 2017;114:2573–89. https://doi. org/10.1016/j.egypro.2017.03.1415.

[32] Carbon Clean. Carbon Clean provides India's first blast furnace carbon capture plant 2021. https://www.carbonclean.com/news/carbon-capture-plant-for-tata-st eel (accessed January 29, 2024).

[33] Tata Steel. Tata Steel commissions India's first plant for CO2 capture from Blast Furnace gas at Jamshedpur 2021. http://www.tatasteel.com/media/newsroo m/press-releases/india/2021/tata-steel-commissions-india-s-first-plant-for-co2-ca pture-from-blast-furnace-gas-at-jamshedpur/ (accessed January 29, 2024).

[34] TERC. Carbon Capture Equipment 2023. https://terc.ac.uk/equipment/carbon -capture-equipment/ (accessed December 18, 2023).

[35] ECCSEL ERIC. Amine Capture Plant 2023. https://www.eccsel.org/catalogue/313 (accessed December 18, 2023).

[36] Akram M, Ali U, Best T, Blakey S, Finney KN, Pourkashanian M. Performance evaluation of PACT Pilot-plant for CO2 capture from gas turbines with Exhaust Gas Recycle. Int J Greenhouse Gas Control 2016;47:137–50. https://doi.org/10.1016/ j.ijggc.2016.01.047.

[37] Akram M, Milkowski K, Gibbins J, Pourkashanian M. Comparative energy and environmental performance of 40 % and 30 % monoethanolamine at PACT pilot plant. Int J Greenhouse Gas Control 2020;95:102946. https://doi.org/10.1016/j. ijggc.2019.102946.

[38] Akram M, Jinadasa MHWN, Tait P, Lucquiaud M, Milkowski K, Szuhanszki J, et al. Application of Raman spectroscopy to real-time monitoring of CO2 capture at PACT pilot plant; Part 1: Plant operational data. Int J Greenhouse Gas Control 2020;95:102969. https://doi.org/10.1016/j.ijggc.2020.102969.

[39] Tait P, Buschle B, Milkowski K, Akram M, Pourkashanian M, Lucquiaud M. Flexible operation of post-combustion CO2 capture at pilot scale with demonstration of capture-efficiency control using online solvent measurements. Int J Greenhouse Gas Control 2018;71:253–77. https://doi.org/10.1016/j.ijggc.2018.02.023.

[40] Akram M, Skylogianni E, Veronezi Figueiredo R, Monteiro J, Grimstvedt A, Vevelstad SJ, et al. Comparison of TERC and TNO's LR2 CO2 capture rigs for normal and accelerated degradation 2022. Doi: 10.2139/ssrn.4279777.

[41] Rose JW, Cooper JR. Technical Data on Fuel. 7th Edition. The British National Committee, World Energy Conference; 1977.

[42] Heeley A. Typical iron and steel making process emission compositions 2024.

[43] Aspen Technology I. Rate-Based Model of the CO2 Capture Process by MEA using Aspen Plus Aspen Plus. 2008.

[44] Zhang Y, Chen CC. Modeling CO2 absorption and desorption by aqueous monoethanolamine solution with aspen rate-based model. Energy Procedia 2013; 37:1584–96. https://doi.org/10.1016/J.EGYPRO.2013.06.034.

[45] Hikita H, Asai S, Ishikawa H, Honda M. The kinetics of reactions of carbon dioxide with monoethanolamine, diethanolamine and triethanolamine by a rapid mixing method. Chem Eng J 1977;13:7–12. https://doi.org/10.1016/0300-9467(77) 80002-6.

[46] Pinsent BRW, Pearson L, Roughton FJW. The kinetics of combination of carbon dioxide with hydroxide ions. Trans Faraday Soc 1956;52:1512. https://doi.org/ 10.1039/tf9565201512.

[47] Song Y, Chen CC. Symmetric electrolyte nonrandom two-liquid activity coefficient model. Ind Eng Chem Res 2009;48:7788–97. https://doi.org/10.1021/IE9004578.

[48] Gross J, Sadowski G. Perturbed-chain SAFT: An equation of state based on a perturbation theory for chain molecules. Ind Eng Chem Res 2001;40:1244–60. https://doi.org/10.1021/IE0003887/ASSET/IMAGES/MEDIUM/ IE0003887E00079.GIF.

[49] Gross J, Sadowski G. Application of the perturbed-chain SAFT equation of state to associating systems. Ind Eng Chem Res 2002;41:5510–5. https://doi.org/10.1021/ IE010954D/ASSET/IMAGES/LARGE/IE010954DF00010.JPEG.

[50] Zhang Y, Chen H, Chen CC, Plaza JM, Dugas R, Rochelle GT. Rate-based process modeling study of CO2 Capture with aqueous monoethanolamine solution. Ind Eng Chem Res 2009;48:9233–46. https://doi.org/10.1021/IE900068K/ASSET/ IMAGES/LARGE/IE-2009-00068K_0022.JPEG.

[51] Madeddu C, Errico M, Baratti R. CO2 Capture by Reactive Absorption-Stripping: Modeling, Analysis and Design. Cham: Springer International Publishing; 2019. Doi: 10.1007/978-3-030-04579-1.

[52] Lewis WK, Whitman WG. Principles of gas absorption. Ind Eng Chem 1924;16: 1215–20. https://doi.org/10.1021/IE50180A002/ASSET/IE50180A002.FP.PNG_ V03.

[53] Errico M, Madeddu C, Pinna D, Baratti R. Model calibration for the carbon dioxide-amine absorption system. Appl Energy 2016;183:958–68. https://doi.org/ 10.1016/J.APENERGY.2016.09.036.

[54] Kucka L, Müller I, Kenig EY, Górak A. On the modelling and simulation of sour gas absorption by aqueous amine solutions. Chem Eng Sci 2003;16:3571–8. https:// doi.org/10.1016/S0009-2509(03)00255-0.

[55] Onda K, Takeuchi H, Okumoto Y. Mass transfer coefficients between gas and liquid phases in packed columns. J Chem Eng Japan / JCEJ 1968;1:56–62. https://doi. org/10.1252/jcej.1.56.

[56] Chilton TH, Colburn AP. Mass transfer (absorption) coefficients: prediction from data on heat transfer and fluid friction. Ind Eng Chem 1934;26:1183–7. https:// doi.org/10.1021/IE50299A012/ASSET/IE50299A012.FP.PNG_V03.

[57] Mores P, Scenna N, Mussati S. A rate based model of a packed column for CO2 absorption using aqueous monoethanolamine solution. Int J Greenhouse Gas Control 2012;6:21–36. https://doi.org/10.1016/J.IJGGC.2011.10.012.

[58] Stichlmair J, Bravo JL, Fair JR. General model for prediction of pressure drop and capacity of countercurrent gas/liquid packed columns. Gas Sep Purif 1989;3: 19–28. https://doi.org/10.1016/0950-4214(89)80016-7.

[59] McNulty K, Hsieh C. Hydraulic Performance and Efficiency of Koch Flexipac Structured Packings. AIChE National Meeting, Los Angeles, CA: 1982.

[60] Zhu K, Yue C, Wei Z, Huang J, Hu M, Ji Y, et al. Experimental and thermodynamic Investigation on CO2 absorption in aqueous MEA solution. Adv Mater Sci Eng 2022;2022:6278342. https://doi.org/10.1155/2022/6278342.

[61] Rieder A, Unterberger S. EnBW's post-combustion capture pilot plant at heilbronn-results of the first year's testing programme. Energy Proc 2013;37:6464–72. https://doi.org/10.1016/j.egypro.2013.06.576.

[62] Gibbins J, Lucquiaud M. BAT Review for New-Build and Retrofit Post-Combustion Carbon Dioxide Capture Using Amine-Based Technologies for Power and CHP Plants Fuelled by Gas and Biomass as an Emerging Technology under the IED for the UK Ver.1.0. UKCCSRC 2021.

[63] Weiland R, Hatcher N, Alvis S. Pinched Performance: Part 1. Digital Refining 2015.

[64] Hatcher N, Alvis S, Weiland R. Gas treating simulation – a holistic perspective part 2: carbon capture. Digital Refining 2013.

[65] Hatcher N, Alvis S, Weiland R. Gas treating simulation — a holistic perspective part 3: co2 removal in an LNG plant. Digital Refining 2013.

[66] Gibbins J. Amine stripper temperature profile a key to optimising net-zero performance in post-combustion carbon capture plants | LinkedIn. LinkedIn 2023. https://www.linkedin.com/pulse/amine-stripper-temperature-profile-key -optimising-net-zero-gibbins/ (accessed January 28, 2024).

[67] Michailos S, Gibbins J. A modelling study of post-combustion capture plant process conditions to facilitate 95–99% CO2 capture levels from gas turbine flue gases. Front Energy Res 2022;10.

[68] Michailos S, Gibbins J. Effect of stripper pressure and low lean loadings on the performance of a PCC plant for 99% CO2 capture level. SSRN Electron J 2022. https://doi.org/10.2139/ssrn.4283827.